

AUTOMATIC FAULT DIAGNOSIS OF ROTATING MACHINERY**A. Oulmane, A.A.Lakis* and N. Mureithi**Department of Mechanical Engineering, École Polytechnique de Montréal, C.P.
6079, Succ. Centre-Ville, Montréal, Québec, Canada H3C 3A7

ABSTRACT: *A key challenge to successful implementation of Time-Frequency (TF) analysis for machine diagnosis is the development of an accurate and consistent method to interpret the images so that they truly reflect machine condition. In this paper, the time-frequency domain is used to study signals from industrial bearings. Examination results are presented as TF images. A Fuzzy logic approach is developed to classify Fourier Descriptors obtained from the time-frequency images so that the fault can be automatically identified. The analysis and results of experimental data indicate that bearing faults can be correctly classified using the developed method.*

KEYWORDS: Time-Frequency Analysis, Fourier Descriptors, Fuzzy Logic Method, Failure Diagnosis, Diagnostics, Rotating Machinery.

INTRODUCTION

Monitoring of machinery is currently used as a predictive maintenance tool. Its primary purpose is safety, but it is also expected to detect the beginning of a defect and follow its development over time. Such early detection makes it possible to plan and schedule repairs for a suitable time in order to avoid production interruptions. Analysis of signals to extract hidden information is known as signal processing. Signal processing methods are the principal tools used in the diagnostics of machinery. Modern technology is progressing rapidly and machinery diagnostics plays a major role in plant maintenance. For this reason, it is essential to take advantage of a new generation of more powerful methods of signal analysis. These methods, called time-frequency representations, make it possible to analyze non-stationary or cyclo-stationary signals [1-4].

If a random signal is not stationary, its correlation function usually depends on time and its spectral density. Representations in time-frequency (RTF), that describe the frequency progress in time, can be used to analyze such cases.

The most immediate representation is the Spectrogram (STFT), which carries the conventional Fourier Transform of one part of the signal; the part moving along the time axis. The precise formulation is [5]:

$$R(t, f) = \int x(u).w(u - t).e^{-i2\pi fu} du \quad (1)$$

The role of the window $w(t)$ is to isolate a neighborhood of length L of the point t , in which the frequency contents are analyzed. In spite of its single and intuitive aspect, this transformation is bijective, and therefore contains all the information of the signal. It is understood that there is a compromise between the length L of $w(t)$, which induces a frequency resolution $1/L$, and the capacity of the Time Frequency distribution to handle variations in modulation speed.

The STFT representation is not the only distribution capable of representing the evolutionary spectral properties of a signal. The Wigner-Ville distribution is the most widely-used member of the class of representations called class of Cohen.

The following distributions result from various choices of the Kernel $\Phi(\theta, \tau)$ [5]:

- $\Phi(\theta, \tau)=1$ gives the Wigner-Ville representation
- $\Phi(\theta, \tau) = e^{i\theta\tau/2}$ gives the Rihaczek representation
- $\Phi(\theta, \tau) = e^{i\theta|\tau|/2}$ gives the Page representation
- $\Phi(\theta, \tau) = e^{-\theta^2\tau^2/\sigma}$ gives the Choi-Williams representation, for which the choice of parameter σ reduces interference terms.

Time-scale representations are also bilinear representations, but they are originally designed for a different purpose: for a complex signal, wave forms which have undergone temporal translations and contraction are sought, and it is natural to look for a correlation between the signal and these dilated and translated forms. To facilitate this, the Continuous Wavelet transformation is introduced.

Certain difficulties limit the efficiency of machinery diagnosis based on these methods. The majority of engineers have little or no knowledge of advanced signal processing techniques, and it is therefore necessary to have user-friendly software. This software must include both advanced and traditional methods of signal analysis in order to automatically identify the faults in different machinery components (such as bearings, shafts, gears...). Automated visual examination systems needed to identify and classify probable defects from images must be rapid and rigorous.

In this paper, thresholding and an 8-connectivity algorithm were applied to an image generated using time-frequency analysis. In addition, a Fuzzy logic method is used to classify a Fourier descriptor found in the image to detect faults in an industrial bearing.

Image Pre-Processing Algorithm

The fault detection method proposed in this work includes an image processing portion, which is applied to enhance information that is extracted from numerical images.

This section presents a short description of two basic image processing methods used in this research: threshold filtering and connectivity algorithms. Threshold filtering converts a continuous gray scale image into a two-or-more-level image such that the concerned contours are separated from the background. Shape images obtained from real operating systems are often corrupted with noise, and as a result the shape obtained from the threshold usually has noise around its boundary. A de-noising process is therefore applied using a classical wavelet transform to decompose the signal, remove noise from components and then reconstruct it [6]. This eliminates isolated pixels and small isolated regions or segments.

In digital imaging characterized by a grid, a pixel can either have a value of 1, when it is part of the pattern, or 0, when it is part of the background. In our case, a pixel is 4-attached to its four neighbors, and 8-attached to its eight neighbors [7]. The most important process is finding a set of connected components in the time-frequency analysis image, because all points in this

set form a candidate area to represent a contour. An example of pre-processing is shown in Figure 1.

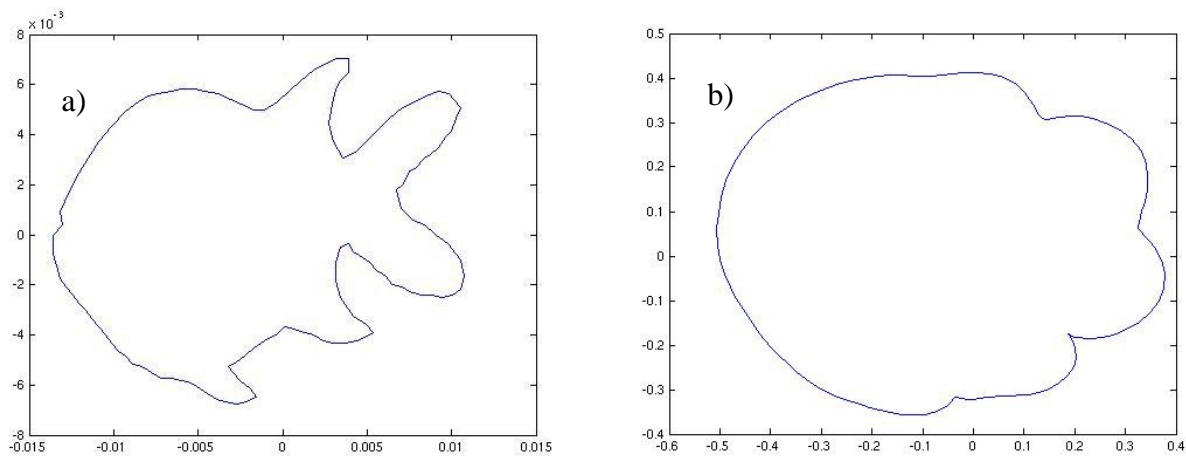


Figure 1-Pre-processing example; a) original image and b) Traced shape [14].

Fourier descriptors

Fourier descriptors (FD) are generally used to represent the outline of an object. An outline (contour) consists of a set of coordinates (x_i, y_i) , and all coordinates are considered as a part of the complex plane $S[n] = x[n] + iy[n]$ as depicted in Figure 2.

The FDs are used to describe the shape of every silhouette located in an image. Their principal benefit is invariance to rotation, translation and scaling of the detected contour.

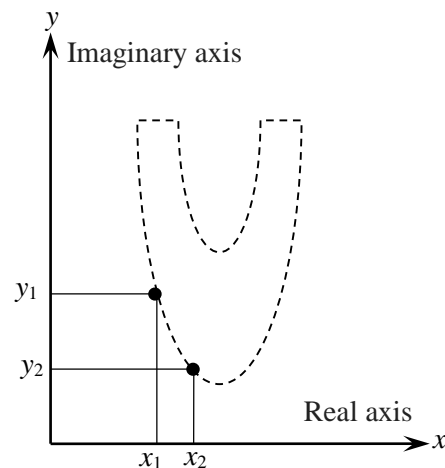


Figure 2- Representation of a contour as a sequence of complex points.

In object recognition methods, silhouette descriptors are found using the entire pixel inside a contour area. Contour descriptors are used in the same region to define the form of an object.

Preprocessing is used to extract the contour information (coordinates of the contour), from the object with invariant descriptors.

The silhouette of the object is then found using a connectivity contour method to obtain the final boundary coordinates of the form. The block diagram for preprocessing and recognition is shown in Figure 3.

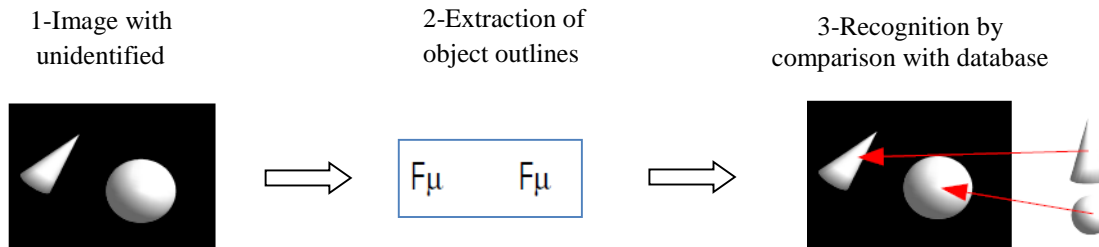


Figure 3-Object recognition using shape information [14].

Classifying the time–frequency images using a Fuzzy logic Algorithm

Introduction of Fuzzy logic: Fuzzy Logic (FL) is a popular approach to derive soft classifiers. It extends conventional Boolean logic using a concept of partial truth for values between “0” and “1”, which correspond to “totally true” and “totally false”, respectively. [20].

The FL method uses mathematical tools (fuzzy sets) to model approximate reasoning when data is imprecise, uncertain, vague, and incomplete.

Clustering data using Fuzzy C-Means (FCM): The FCM is a method of grouping that permits one data set to belong to double or several clusters. The main objective of clustering is to recognize regular groupings of data from an important set of data [21-22].

Classifying the Fourier descriptors with Fuzzy C-Means: Suppose we have a data set: $\{X_1 \dots \dots X_N\}$, that we want to separate into C fuzzy clusters. This requires computing C centers of the group and generating a connection matrix U . This membership matrix is a $C \times N$ matrix, where C is the total number of clusters and N is the data sample quantity. Each membership matrix column involves C membership values corresponding to each data sample [19].

An ideal distribution using fuzzy C-Means is generated by reducing the global least squared errors function $J(U, v)$ [17]:

$$J_m(U, v) = \sum_{k=1}^N \sum_{i=1}^C (U_{ik})^m \|X_k - v_i\|^2 \quad (2)$$

where $X = (X_1 \dots \dots X_N)$ is the set of data, C is the number of cluster centers (C between 2 and N), and m is the increment of weighting exponent ($1 \leq m < \infty$).

$\|X_k - v_i\|^2 = \sum_{j=1}^N (X_{jk} - v_{ji})^2$; where $\|X_k - v_i\|$ is the Euclidean metric.

N is the number of datasets.

$v = [v_{ji}] = [v_1, \dots \dots v_C]$ is the matrix of cluster centers;

v_i is the cluster center for subset i ;

U_{ik} is the value of fuzzy membership of sample k in group i ;

$U = [U_{ik}]$: Fuzzy C-partition matrix for the data set X .

$U \in R^{C \times N} \forall i, k: 0 \leq U_{ik} < 1$.

At points where $\sum_{i=1}^C U_{ik} = 1$,

$$0 < \sum_{k=1}^N U_{ik}$$

In this paper, the Fuzzy Logic method is applied to Time-Frequency images and a set of Fourier descriptor values for each object found in the image are introduced as input data to the FCM algorithm classification. In reference [23], an *Application of Fourier Descriptors and Fuzzy Logic for classification of a Radar Subsurface Image* was developed specifically for recognition of Archeological artifacts. The buried artifacts in these images appear in the form of hyperbolas due to radar backscatter from the artifacts. The procedure consists of using Fourier Descriptors and a Fuzzy C-Mean Classifier to separate two classes of hyperbola/non-hyperbola objects from the sub-surface images [23]. Many other authors have applied this method in different fields, such as: a) Gabor B, a study in which the author investigates automatic object recognition (Fourier Descriptors and fuzzy logic) in unconstrained environments in order to resolve a problem of an inexact fit from the source map to the final digital product [24].

b) Abdul Salam. T. H et al; the authors use invariant Fourier Descriptors to recognize, identify and classify objects (with invariant moments, fuzzy logic techniques etc...) from a 2D image [25];

c) Sérgio Oliveira studied authors that implement procedures for classification in intelligent systems using Fourier descriptors to define the contour of objects. Intelligent systems incorporating FL (fuzzy sets) have proven highly effective using only two Fourier descriptors, even when these are calculated using very few points to define the object's contour obtained from an image taken by a smart camera [26].

d) Wang et al. present a fuzzy logic-based image retrieval system founded on color and shape features. The authors adopt Fourier descriptors and moment invariants to describe the shape feature of a binary image [27].

In the present paper, an intelligent detection and classification system for industrial signals based on analysis of the time-frequency domain is proposed. A set of significant Fourier descriptors are chosen as the features of an array vector that describes the contour of a time-frequency image. A comparison procedure is implemented between the latter and a dictionary created especially for this purpose. The nearest neighbor process determines the Euclidean distances between the sample array vectors and each new product. The product is classified as non-defective if the nearest prototype is a non-defective product model. Otherwise the product is classified as defective.

Experimental Setup

Bearing characteristic frequencies: A rolling element bearing typically contains two rings, an interior and an exterior race with a set of balls retained in a cage. This prevents any contact

between rollers and also provides uniform spacing (Figure 4). There are many causes of bearing failures, including material flaws, lubricant failure, misaligned load, excessive contact stress, etc. In almost all cases the malfunction occurs due to a defect in the inner race, outer race or rolling elements. A vibration analyst can often detect/predict failures by collecting enough information about the frequencies emitted by a defective bearing.

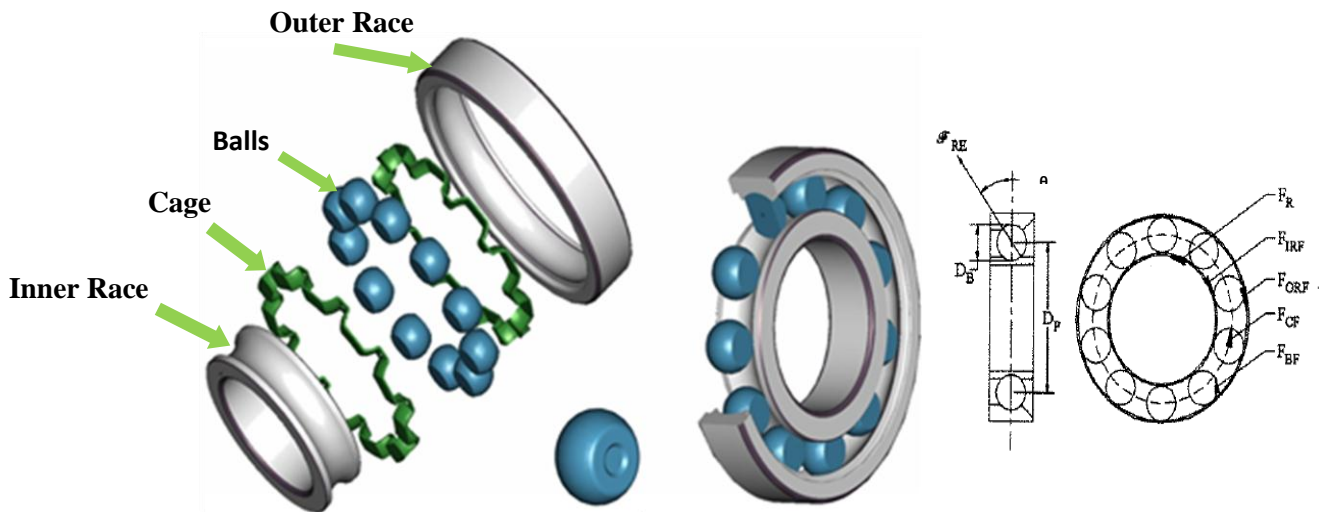


Figure 4-Different components of the bearing [Schoen *et al.*].

Three important frequencies that defective bearing can generate are:

- 1- Ball/roller pass frequency of the outer race (BPFO): this frequency occurs when each Ball/roller passes over the defective location in the outer race and can be calculated using the formulas in Table1.
- 2- Ball/roller pass frequency of the inner race (BPFI): this frequency occurs when each Ball/roller passes over the defective location in the inner race.
- 3- Two times Ball/roller spin frequency (BSF): this frequency equals twice the spinning frequency of the Ball/roller. This occurs due to a single fault in roller contacts of the inner and outer rings.

To calculate the BPFO, BPFI and BSF of a bearing, geometry and rotational speeds of the bearing are needed.

Table 1: Fault characteristic frequencies of a ball bearing system.

<i>Frequencies</i>	<i>Formulas</i>
Cage fault (F_{CF})	$F_{CF} = \frac{1}{2} F_R \left(1 - \frac{D_B \cos \theta}{D_P} \right)$
Outer raceway fault (F_{ORF})	$F_{ORF} = \frac{N_B}{2} F_R \left(1 - \frac{D_B \cos \theta}{D_P} \right)$
Inner raceway fault (F_{IRF})	$F_{IRF} = \frac{N_B}{2} F_R \left(1 + \frac{D_B \cos \theta}{D_P} \right)$

Ball fault	$F_{BF} = \frac{D_P}{2D_B} F_R \left(1 - \frac{D_B^2 \cos^2 \theta}{D_P^2} \right)$
Where; F _R is spindle speed revolution, D _B : ball diameter, D _P : distance between the center of two opposing balls, N _B : quantity of balls and θ: ball contact angle.	

Data Acquisition

First case study: This case study presents the design of an experimental test rig to measure vibration signal responses of faulty rotating machinery components (simulated faults). The test rig is designed to detect typical rotating machinery faults such as a damaged bearing, mass imbalance and a gear fault. Since our diagnosis procedure is based on vibration signals, its reliability depends on how well the simulated signals reflect those that are obtained from real systems used in industry. We also need to adequately control the nature of the vibrations simulated on the test rig, i.e. eliminate all potential sources of noise. For these reasons, design of the test rig was carried out following a strict set of procedures. First, it was necessary to define the components to be tested and the test parameters, including speed and the loads to be applied on tested components. Once faulty components were identified, a common way to simulate faults similar to those usually encountered in industry was proposed. Finally, instrumentation of the test rig was considered.

In many previous works, test rigs were made of bearings, gears, and a disk or flywheel mounted on a rotating system driven by an electric motor.

Our test rig is a rotating system consisting of a shaft supported at each end by SKF Plummer block bearings. These are connected to a gearbox system through a belt transmission system. The whole system is driven by a 2 HP electrical motor at 3600 rpm nominal speed mounted on a set of two 67 lb/ft H-beams. The motor is coupled to the rotating system using a standard elastomeric connector that can sustain angular misalignment and absorb some unwanted vibration coming from the motor. The test rig is 210 mm wide and 1750 mm long.

An unbalanced flywheel is mounted on the shaft. This arrangement and the belt transmission system provide loads on the bearings. The gears are mounted on shafts which are supported by bearings at each end. All bearings (those of the rotating system and those of the gearbox) are mounted on adapter sleeves and can be easily dismantled for replacement. The speed ratio of the gear transmission is 1.16, whereas the ratio for the belt transmission is 1.06.

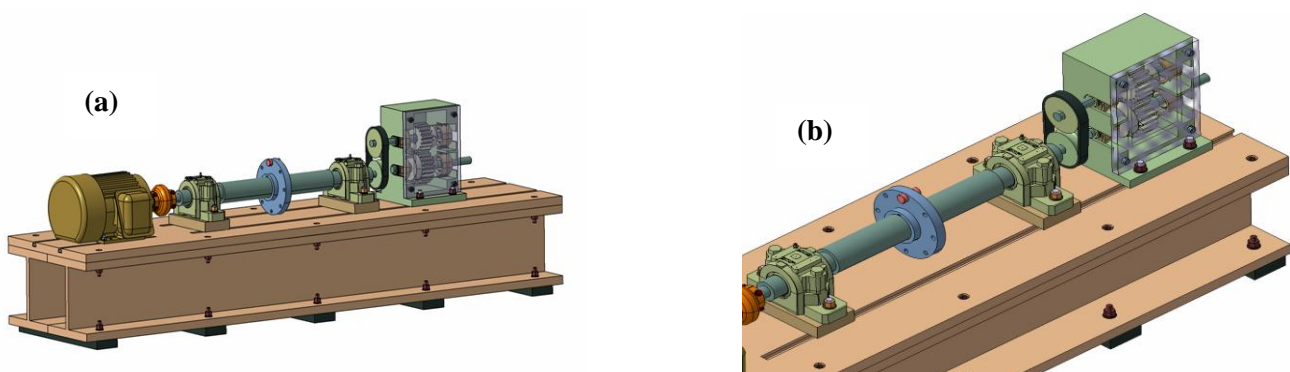


Figure 5-Test rig for the analysis Machinery Diagnostics laboratory at École Polytechnique of Montreal, (a) isometric view and (b) Zoom isometric view.

While the motor runs at its nominal rotational speed of 3600 rpm, output shaft of the belt transmission rotates at 3400 rpm and the output shaft of the gear transmission rotates at 2900 rpm. If the belt and gear transmissions are used for speed multiplication, their output speeds will be 3800 and 4400 rpm, respectively. The maximum speed that can be reached on this test rig is therefore 4400 rpm. The gearbox unit, the imbalance flywheel, and the shafts were custom designed for this test rig. All other components were purchased from suppliers.

Table 2: Test rig specifications.

Components	Specifications	Manufacturers
Base	2 H-Beams W8×8 67lb/ft	Prometo
Motor	2Hp, 3600rpm, 575Volts	Toshiba
Couplings	7/8inch - 1inch	Rex Omega
Bearing House	SNL 510 - H310 - 1210EKTN9	SKF Canada

Pratt & Whitney bearing Tests: The goal of the present work is to demonstrate that the developed procedure can diagnose any faulty condition in rotating machinery. This is done by analyzing the vibration response of components such as Pratt & Whitney bearings on the test rig. An adapted version of the original test rig is presented in the Figures. Since Pratt & Whitney bearings are not available on the market, a bearing housing of appropriate dimensions was designed. The gearbox transmission was replaced by the custom-made bearing housing and an SKF Plummer block bearing. These two units are used to support the shaft connected to the output of the belt transmission system.

The tested bearing is now loaded by the belt transmission system. A set of internal and external adapter sleeves was designed to accommodate all bearing dimensions required by Pratt & Whitney.

The details of the design are shown in Figures 6 and 7. The housing adapter sleeves enable changing the bearings without disassembly of the whole system. Only the central part shown on the cover of the bearing housing needs to be removed and reinstalled.

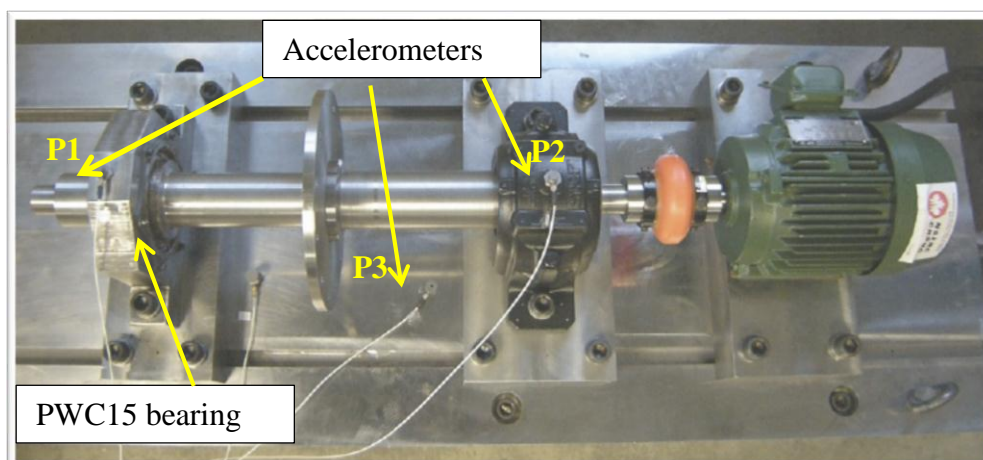
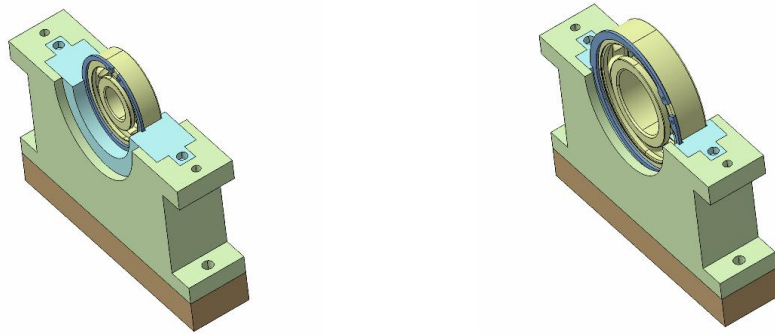
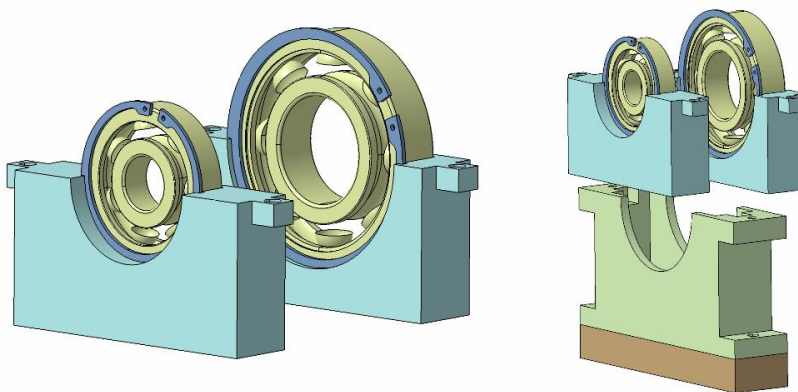


Figure 6-Test setup with PWC100#5 bearing mounted on the shaft.



(a) Bearing housing with smaller bearing, (b) Bearing housing with larger bearing



(c) Housing adapter sleeves

(d) Replacing bearings inside the housing

Figure 7- Test rig adapted for Pratt & Whitney bearings.

Test specifications: Using the in-house Software TF-Analysis, spectral analysis was undertaken to detect possible faults in the industrial bearing provided by Pratt and Whitney, see Figure 7. The tests on the bearing were carried out in the Machinery Diagnostics Laboratory at École Polytechnique of Montreal, according to specifications provided by Pratt and Whitney.

Tests were carried out at 3 different rotating speeds (S1, S2 and S3, see Table 3). Data was gathered at a sampling frequency of 50 kHz, with 5 minute recordings at each speed. The acceleration and deceleration stages were recorded as well. See Figure 8 for the test sequence

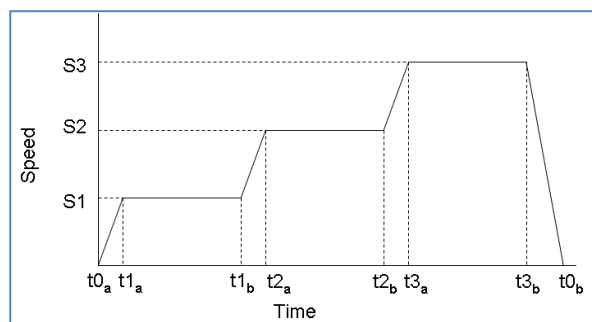


Figure 8-Test speed scheme.

Table 3: Test speed

Speed	Rotating speed (rpm)	Frequency (Hz)
S1	400	6.67
S2	800	13.3
S3	1200	20

Three accelerometers were used; P_1 , P_2 and P_3 (see Figure 6). P_1 is positioned horizontally over the bearing to detect bearing faults. P_2 is positioned vertically on the side of the bearing and detects shaft faults. P_3 is positioned horizontally on the bearing housing (1217K) and is used to monitor this bearing and thus test equipment condition.

In this paper, only the data from P_1 is analyzed while the others are used merely for monitoring and verification of the test equipment.

Technical specification

Bearing parameters

Table 4: Bearing specifications

P&W Bearing ID	PW100 #15 BRG, Roller bearing
Inner diameter	2.7556'' - 2.7559''
Outer diameter	5.9051'' - 5.9055''
Pitch diameter	4.3308''
Width	1.370'' - 1.375''
Contact Angle	n/a
Operating speed 1	400 rpm
Operating speed 2	800 rpm
Operating speed 3	1200 rpm

Calculated defect frequencies

Table 5: Calculated defect frequencies of PW100#5 BRG, Roller bearing.

Frequency rotation	6.67 Hz	13.3 Hz	20 Hz
Defect of cage (F_{CF})	2.64 Hz	5.30 Hz	7.97 Hz
Outer race defect (F_{ORF})	31.67 Hz	63.64 Hz	95.70 Hz
Inner race defect (F_{IRF})	47.76 Hz	95.96 Hz	144.30 Hz
Ball defect (F_{BF})	0.64 Hz	1.29 Hz	1.94 Hz

Second case study: Our second case study involves application of the proposed method to analyze vibration signals collected during a failure of Pratt & Whitney bearing PW100#5. This bearing is part of Pratt & Whitney's aircraft engine PWC100, where it is used to support a gearbox shaft. It has been identified as one of the most problematic components in the engine.

Experimental data was collected from a test rig at the National Research Center in Ottawa. Three bearings of the same type were tested on that test rig.

Steady state and transient signals were recorded at a 50 kHz sampling frequency according to the speed path given in Figure 10.

Note that only data from one of these three bearings; PW100#5 n°3, is analyzed in this paper. Moreover, during the tests the rotational speed was kept low (1,000 and 2,000 rpm) due to excessive noise and risk of damage to the test rig.

Table 6: Geometrical dimensions and rotating speeds for tests performed at NRC on the P&W bearing.

P&W Bearing ID	First	Second	Third
	PW100 #5 Roller bearing	PW100 #5 Roller bearing	PW100 #5 Roller bearing
Inner diameter	2.8347'' - 2.8350''	2.8347'' - 2.8350''	2.8347'' - 2.8350''
Outer diameter	3.9292'' - 3.9272''	3.9292'' - 3.9272''	3.9292'' - 3.9272''
Pitch diameter	3.4165''	3.4165''	3.4165''
Width	0.625'' - 0.630''	0.625'' - 0.630''	0.625'' - 0.630''
Contact Angle	n/a	n/a	n/a
Operating speed 1	25,600 rpm	25,600 rpm	1,000 rpm
Operating speed 2	32,000 rpm	32,000 rpm	2,000 rpm
Operating speed 3	34,200 rpm	34,200 rpm	-



Figure 9-Experimental test setup; NRC test rig.

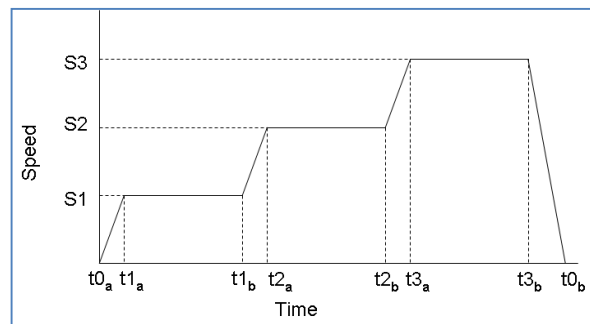


Figure 10-Real rotational speed of the PW100#5 roller bearing: S2=32,000 and S3=34,200 rpm.

As previously shown in Table 1, a number of equations can be used to calculate the fault frequencies of the bearing. Using these formulas, one can compute the defect frequencies of the PW100 #15 bearing, where $D_B = 7.3$ mm, $D_P = 87.8$ mm, $N_B = 12$, and $\theta = 0$.

The theoretical bearing defect frequencies are presented in Table 7 for different rotational speeds. Note that the third bearing was tested at a low speed range of 1,000 to 2,000 rpm due to excessive noise during the speed-up period.

Table 7: Defect frequencies for the PWC100#5 bearing.

Bearing	Rotation Speed (RPM)	Cage fault (FCF) Hz	Inner raceway fault (FORF) Hz	Outer raceway fault (FIRF) Hz	Ball fault Hz
First Bearing	34,200	261.34	3,704.86	3,136.14	3,403.80
	32,000	244.30	3,463.43	2,932.56	3,182.86
	25,600	195.60	2,772.00	2,347.15	2,547.48
Second Bearing	34,200	261.34	3,703.86	3,136.14	3,403.80
	32,000	244.30	3,463.43	2,932.56	3,182.86
Third Bearing	1,000	7.64	108.32	91.71	99.54
Bearing	2,000	15.28	216.58	183.38	199.03

RESULTS AND DISCUSSIONS

Time-Frequency Analysis

As mentioned earlier, the time-frequency analysis method is an alternative method that can be used to detect faults with higher accuracy when bearing defects occur and also to reduce noise effects.

First case study

Visual inspection of the PWC100#5 bearing indicated an outer race fault (Scratches on the outer race bearing surface which is in contact with the balls. Although the defect is small, see Figure 11, it is positioned in the loading zone of the bearing and therefore generates pulses in the vibration signature). Figure 12 shows the spectrum and spectrogram of signals up to 250 Hz gathered by the accelerometer at a rotating speed of 1200 rpm. As is typical with spectral

analysis for the purpose of bearing fault detection, it is expected to have a peak at the same frequency on both diagrams. The spectrum in this case shows a peak around 95 Hz, slightly higher spectral energy can also be observed from the spectrogram around the same frequency. This frequency coincides well with the over-rolling frequency at one point on the outer race of the PWC100#5 bearing, as shown in Table 5 (95.70 Hz).

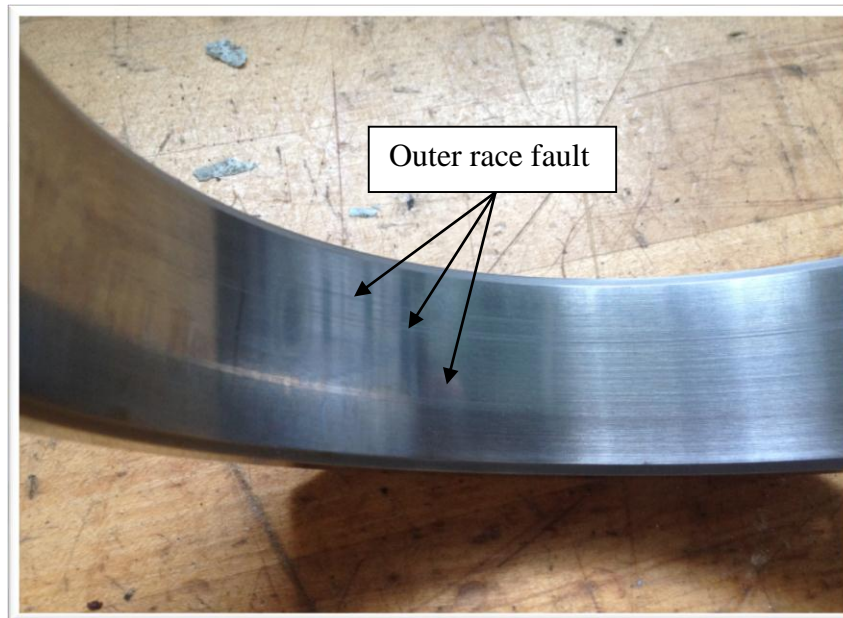


Figure 11-Outer raceway of the tested Pratt & Whitney bearing (PWC100#5)

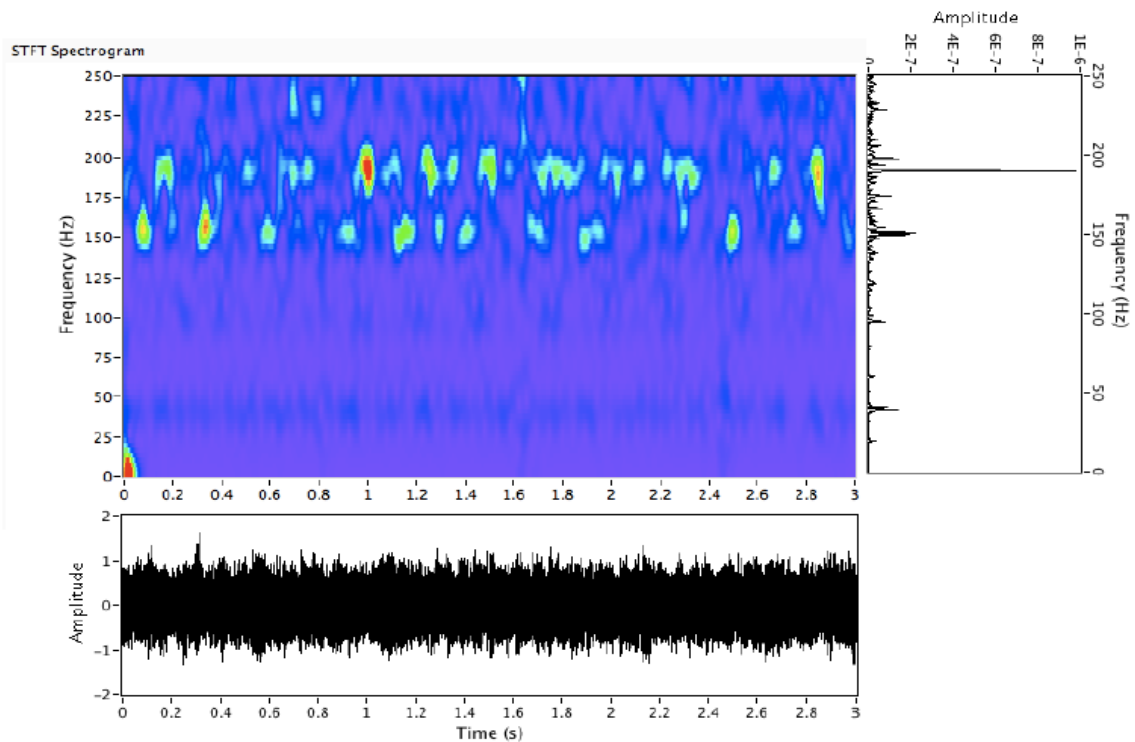


Figure 12-Spectrum and spectrogram of the faulty PWC100#5 bearing.

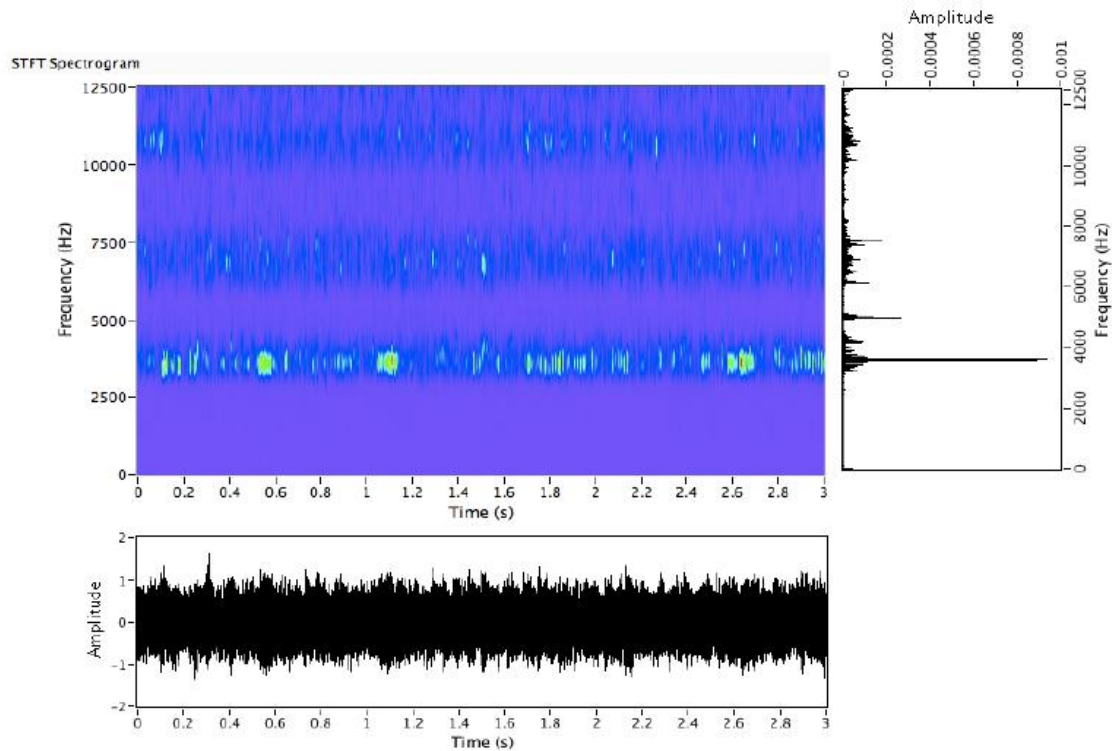


Figure 13-Wide range frequency spectrogram of the faulty PWC100#5 bearing at rotating speed 1200 rpm.

In order for the vibration produced by faulty bearings to be clearly discernible on the spectrogram one needs to look at a broader frequency range. Figure 13 shows the spectrogram and spectrum of the signal up to 12.5 kHz. On the spectrogram, the outer race fault appears as a series of bursts taking place at around 3.5 kHz with an interval equal to the inverse of the outer race fault characteristic frequency (modulation frequency). Figure 14 presents a waterfall plot of the same signal centered on 3.5 kHz and this modulation is confirmed. Indeed, in this figure two main peaks are visible at frequencies 96 Hz and 200 Hz. This indicates that the signal is modulated with a modulation frequency about 96 Hz, which coincides with the outer race fault frequency of the PWC100#5 bearing given in Table 5 (frequency rotation at 20Hz).

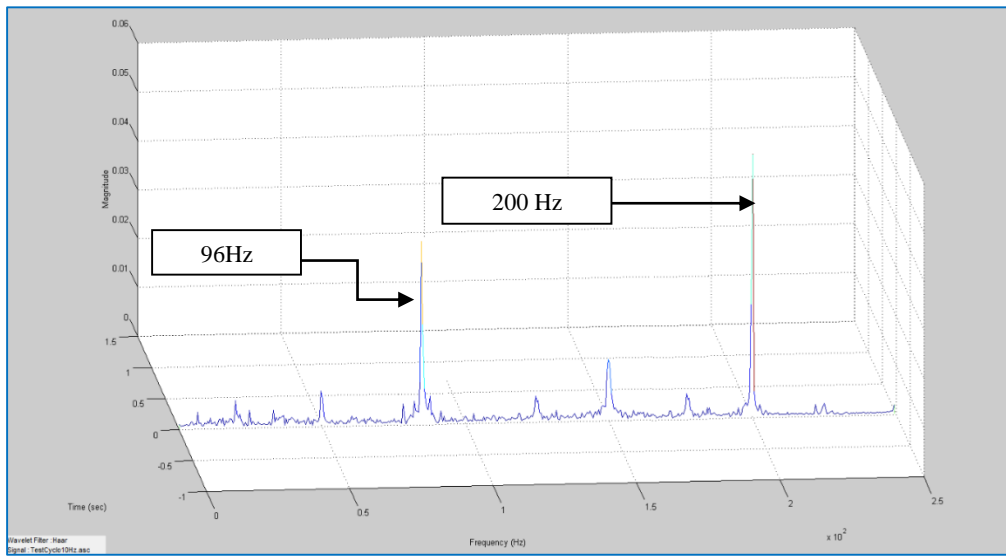
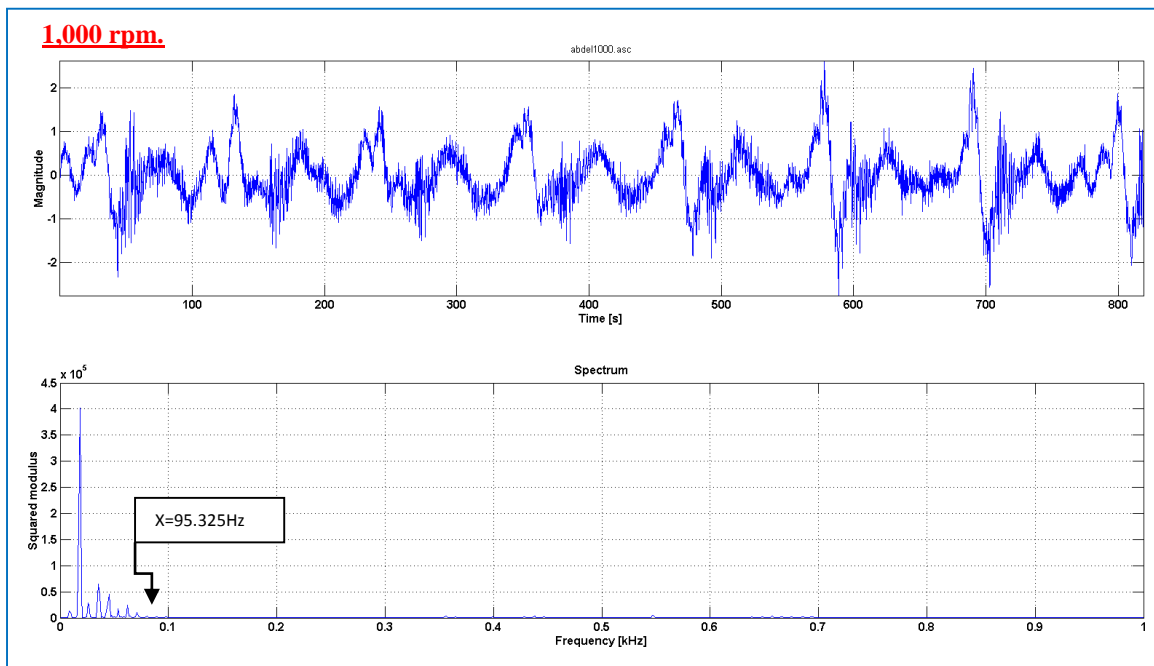


Figure 14-Wide range frequency waterfall plot of the faulty PWC100#5 bearing (at 1200 rpm).

Second case study

Figure 15 shows the signal of the bearing and its spectrum at 1,000 and 2,000 rpm, respectively. The spectrum of the signal shows some tight peaks around 100 and 200 Hz, however it is very difficult to confirm which defects are present in this region.



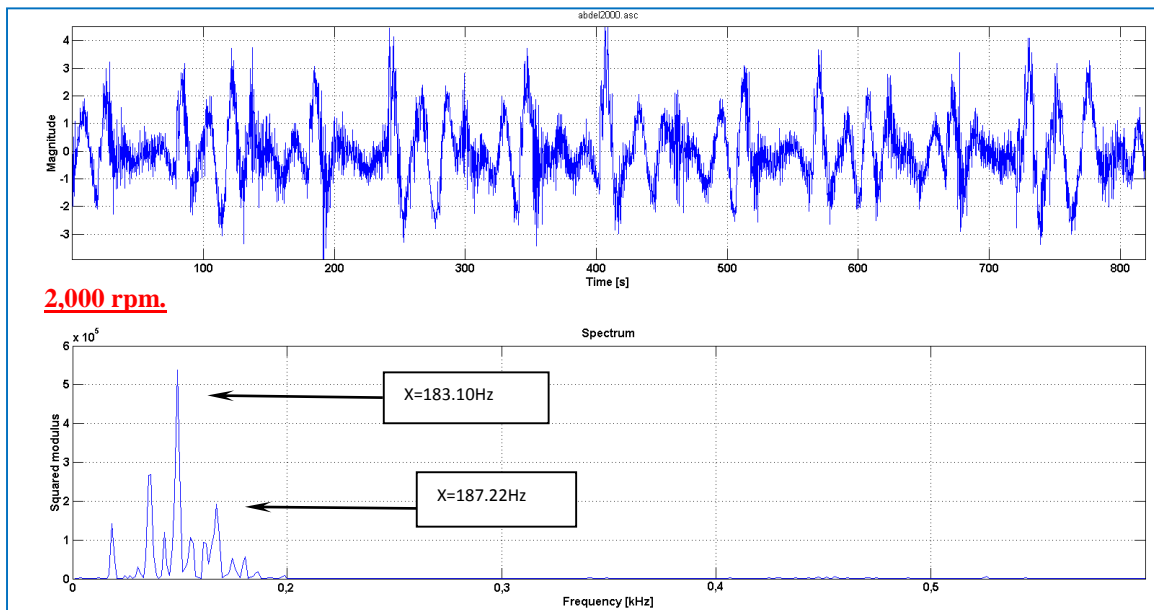
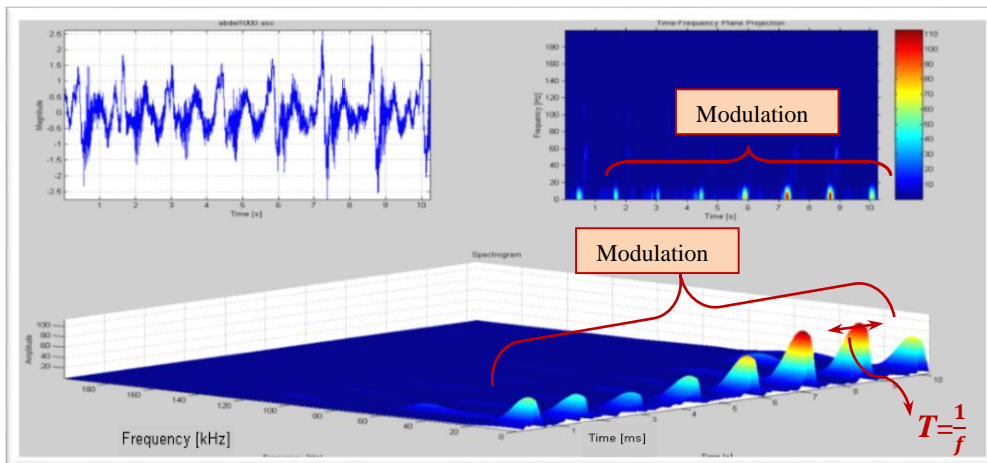


Figure 15-Spectrum signal, bearing PW100 #5 n°3, 1,000 and 2,000 rpm.



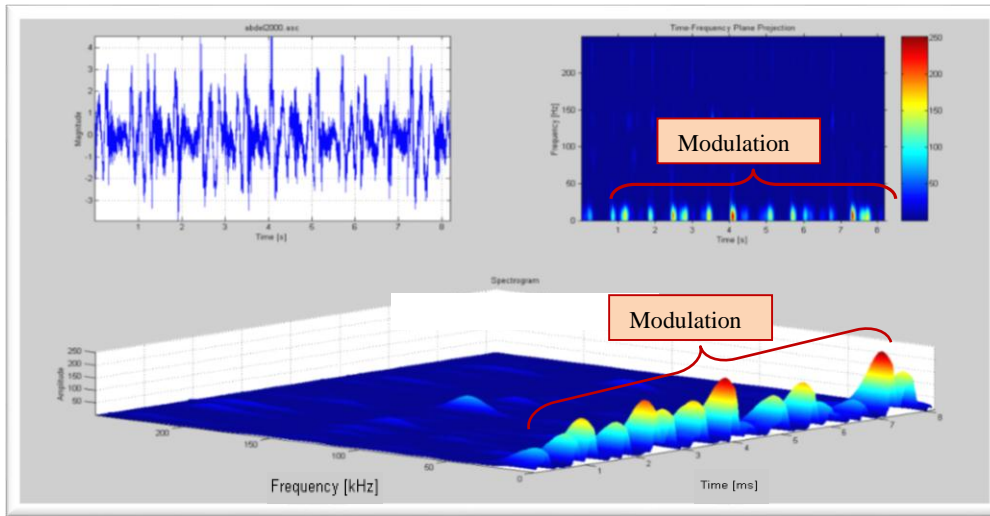


Figure 16-Spectrogram with modulation of bearing n°3, 1,000 and 2,000 rpm.

The time-frequency representation of the signal provided by the spectrogram (Figure 16) shows the amplitude-modulated signal at the inner and outer race fault frequencies and its harmonics. We can easily calculate the time between the two peaks and verify that it is identical to the frequency of the rotating shaft. These particularities observed on the time-frequency representations of the signals recorded at 1,000 and 2,000 rpm allow us to conclude that bearing n°3 has an inner and outer race defect. This diagnosis is confirmed by a visual inspection of the bearing.

Classifying time–frequency images using Fuzzy C-Means and Fourier Descriptors

The analysis in section 7.1 confirms that bearing defects can readily detected using the time-frequency approach. However, the ultimate goal of this work is to diagnose the condition of components in rotating machines automatically. To achieve this, our proposed method involves using a Fuzzy logic classifier (Fuzzy C-Means) and Fourier Descriptors to treat the time–frequency images and identify the faults.

The steps of Fuzzy C-Mean method used in this work can be described in simple terms as follows [21-23]:

Create a set of values for C , m , e (e is a threshold) and generate a loop (iteration) $t = 1$. Then randomly generate an initial membership matrix U with dimensions $N \times C$. The next step is to calculate the center of gravity for each cluster (partition):

$$v_i^{(t)} = \frac{\sum_{k=1}^N (u_{ik}^{(t)})^m x^k}{\sum_{k=1}^N (u_{ik}^{(t)})^m}; i = 1 \dots C \quad (3)$$

Subsequently, the new center of partitioning is used to update the membership matrix:

$$u_{ik}^{(t)} = \frac{1}{\sum_{j=1}^C \left(\frac{d_{ik}}{d_{jk}} \right)^{\frac{2}{m-1}}} \quad (4)$$

Finally, the membership matrix is updated and compared with the preceding matrix:

If $\left\{ \left| u_{ik}^{(t)} - u_{ik}^{(t-1)} \right| \right\} > e$, t is incremented and a new iteration is calculated, in the contrary case, the algorithm is ended.

Outer race defects of bearings PWC #15 and #5 are presented in Figures 17-20 along with the twelve most significant Fourier descriptors. These Figures show; a) the image of an outer race defect of the bearing obtained using a time-frequency representation, b) classification of the objects using the fuzzy logic method and c) Fourier descriptors of one of the objects found in the time-frequency image.

These significant Fourier descriptors are chosen as the first twelve descriptors, that is, C_0, C_1, \dots, C_{11} ; the first elements of the array. This choice is justified because all of the information describing the border of the contour will be found in the lower frequency portion of the signal.

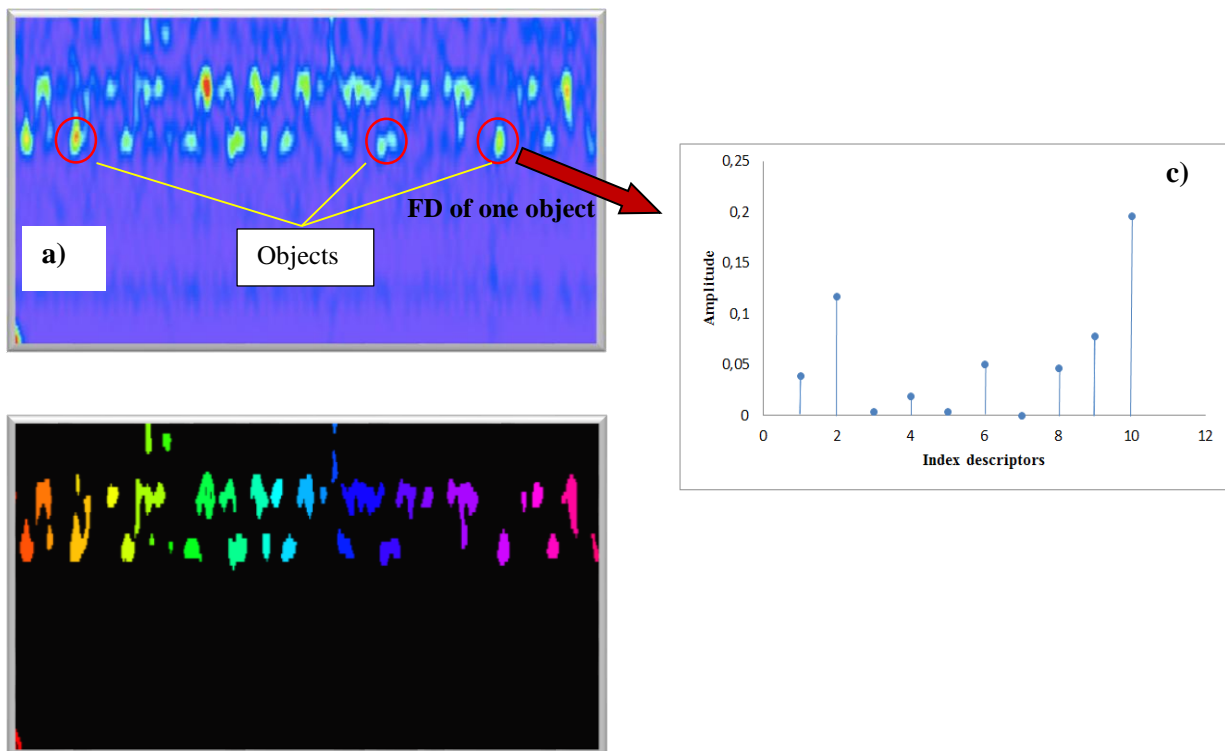


Figure 17 a) Outer race defects of bearing n°15 in time-frequency representation at 400 rpm, b) Fuzzy C-Means classification of the time-frequency image and c) Fourier descriptors of one object

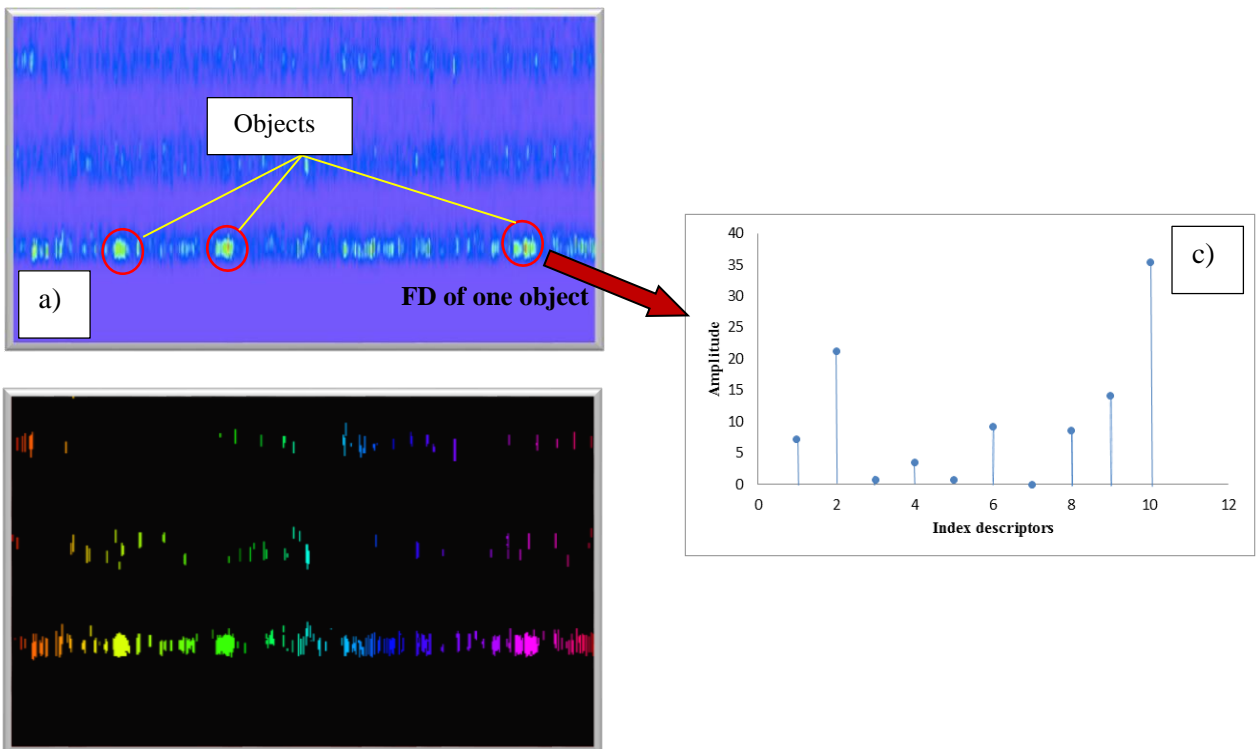


Figure 18 a) Outer race defects of bearing n°15 in time-frequency representation at 800 rpm, b) Fuzzy C-Means classification of the time-frequency image and c) Fourier descriptors of one object.

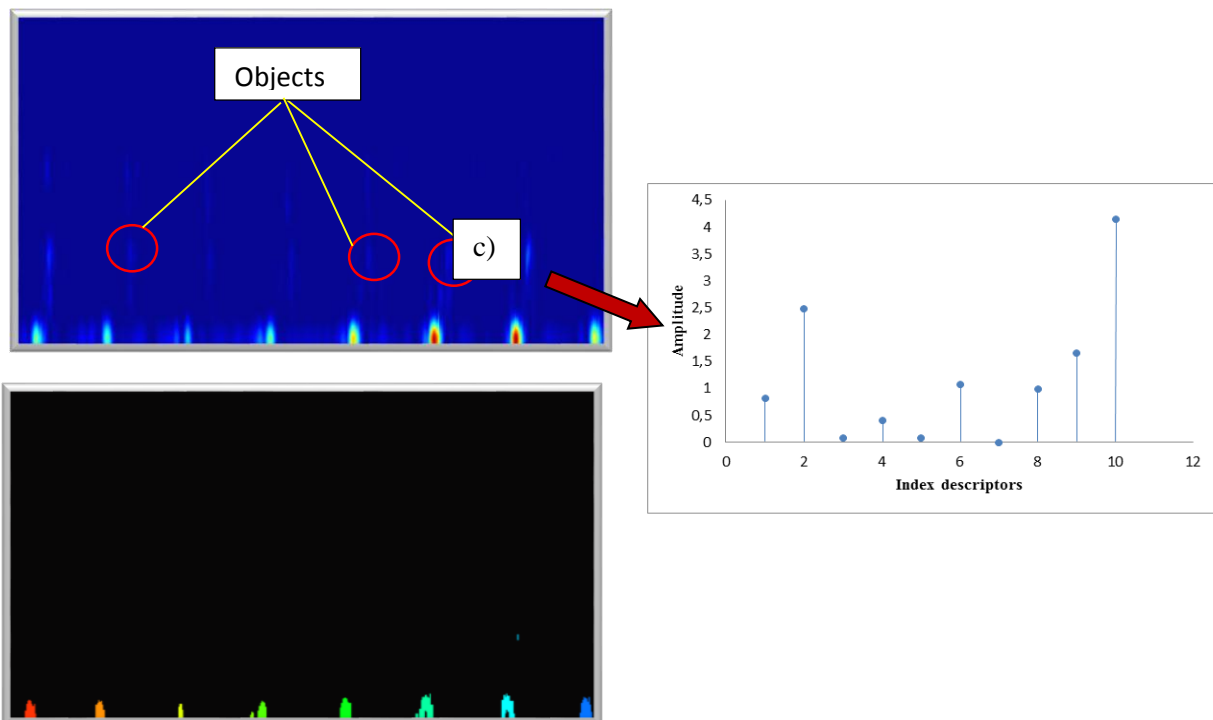


Figure 19 a) Outer race defects of bearing PW100#5 n°3 in time-frequency representation at 1,000 rpm, b) Fuzzy C-Means classification of the time-frequency image and c) Fourier descriptors of one object.

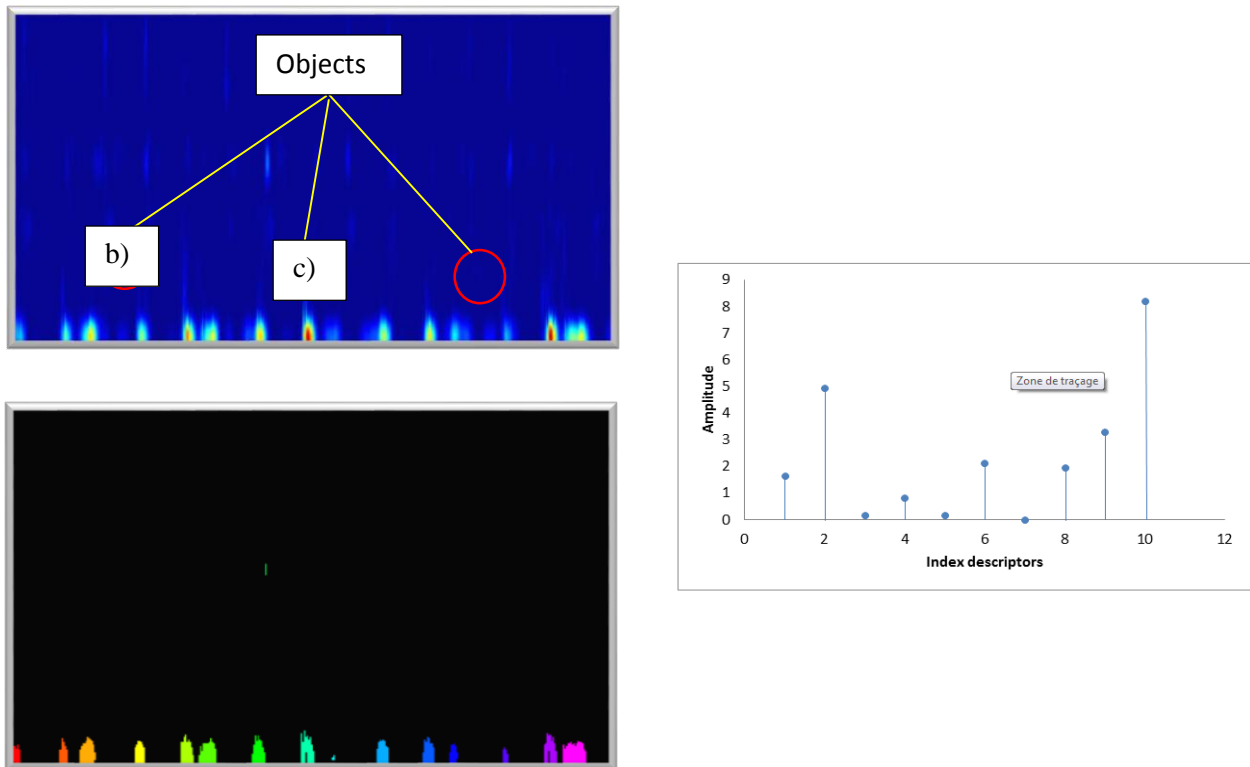


Figure 20 a) Outer race defects of bearing PW100#5 n°3 in time-frequency representation at 2,000 rpm, b) Fuzzy C-Means classification of the time-frequency image and c) Fourier descriptors of one object.

The classification procedure can be described as follows:

- 1- Create a dictionary that contains signals showing the state (whether a defect exists or not) of the bearing. The objective at this stage is to use this dictionary to classify the signals derived from distributions that give the best results for our case. If we state that the best distribution is the one with the largest peak, the image of the top three time-frequency distributions will be selected for this component (bearing) and hence the dictionary is created.
- 2- For a new product, the process to verify whether or not the signal has a fault is as follows. The signal is first processed using the top three distributions retained. In the second step, a series of twelve Fourier descriptors are found for every object in the time-frequency image. These significant Fourier descriptors are chosen as features of the array vector that describe the contour. A comparison procedure is subsequently implemented between the latter and the dictionary (only signals that correspond to the state of the bearing) to identify its state.
- 3- The nearest-neighbor process is used to determine the Euclidean distances between the sample array vectors and those of each new product. The new products are then

classified as non-defective if the nearest prototype is a non-defective model, if not the product is classified as defective.

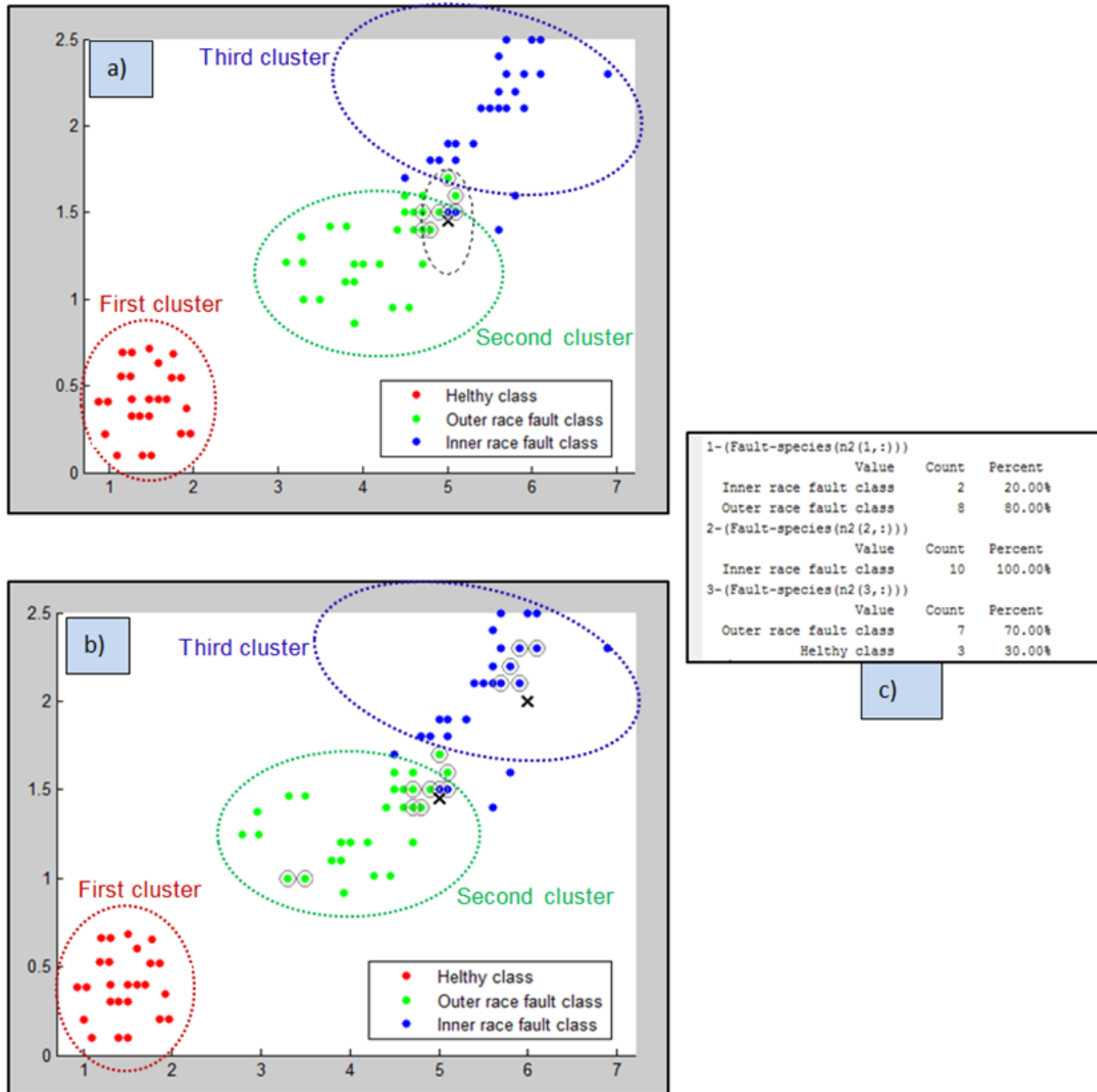


Figure 21-Classification of a Fourier descriptor output for new bearing data a) PW100#5, b) PW100#15 and c) the message describing the performance of the classifier.

The final results of classification using C-Means clustering based on the Fourier Descriptors output data for a new product are shown in Figure 21. Three separate clusters exist in this Figure, which illustrate the positions of defects in different locations. These clusters are classified as follows: healthy class (first class), outer race fault class (second class) and inner race fault class (third class). Results of second and third class are quite close, but they can be divided via classifiers.

Figure 21 illustrates a map of classification for Fuzzy logic clustering of PW100#5 and PW100#15 bearings, respectively. In any one figure, each circle belongs to a defect, and these are separated according to three different class faults. The smallest area of each unidentified sample corresponds to the cluster set in which the fault sample belongs. Figure 21 presents successful classification of the test data. It can be seen that for an unknown test point (x) the classifier associates this point to a specific type of fault class, with a text message indicating the performance of classification.

CONCLUSION

In this paper, an intelligent detection and classification system for industrial signals treated using the time-frequency domain is presented. Results are presented in grey representations. Application of a Fuzzy Logic method using Fourier Descriptors is shown to be capable of automatic defect classification and is successfully applied to identify the condition of a bearing. Performance of the technique is demonstrated using experimental signals. Results confirm good sensitivity and accuracy of the system for automatic detection, localization and assessment of faults.

Acknowledgement

The authors are greatly in debt to Department 9436 of Pratt & Whitney Canada for their generous support and valuable comments. This project was made possible by precious support in the form of a collaborative research and development grant from the Natural Sciences and Engineering Research Council of Canada (NSERC), Bombardier Aeronautics, Pratt & Whitney Canada, and the National Research Council (NRC).

REFERENCES

- W. J. Wang, P. D. McFadden, Early detection of gear failure by vibration analysis I. Calculation of the time-frequency distribution, *Mechanical Systems and Signal Processing*, pp 193-203, 1993.
- F. A. Andrade, I. Esat, M. N. M. Badi, Gearbox fault detection using statistical methods, time-frequency methods (STFT and Wigner-Ville distribution) and harmonic wavelet - A comparative study, in: *Proceedings of COMADEM '99*, Chipping Norton, pp. 77-85, 1999.
- Q. Meng, L. Qu, Rotating machinery fault diagnosis using Wigner distribution, *Mechanical Systems and Signal Processing*, pp 155-166, 1991.
- N. Baydar, A. Ball, A comparative study of acoustic and vibration signals in detection of gear failures using Wigner-Ville distribution, *Mechanical Systems and Signal Processing*, pp 1091-1107, 2001.
- L. Cohen, Time-frequency distribution - a review, *Proceedings of the IEEE*, pp 941-981, 1989.
- D. L. Donoho and I. M. Johnstone, "Idea De-noising in an Orthonormal Basis Chosen from a Library of Bases", *CRAS Paris*, t.319, PP.1322, 1994.
- Rafael C. Gonzalez and Richard E. Woods. *Digital Image Processing*. Addison-Wesley, 1992.
- R. K. Young, *Wavelets Theory and Its Applications*, Kluwer Academic Publishers, Boston, 1993.

- R. Rubini, U. Meneghetti, Application of the envelope and wavelet transform analyses for the diagnosis of incipient faults in ball bearings, *Mechanical Systems and Signal Processing*, pp 287-302, 2001.
- G. Y. Luo, D. Osypiw, M. Irle, On-line vibration analysis with fast continuous wavelet algorithm for condition monitoring of bearing, *Journal of Vibration and Control*, pp 931-947, 2003.
- W. J. Staszewski, G. R. Tomlinson, Application of the wavelet transform to fault detection in a spur gear, *Mechanical Systems and Signal Processing*, pp 289-307, 1994.
- W. J. Wang, P. D. McFadden, Application of wavelets to gearbox vibration signals for fault detection, *Journal of Sound and Vibration*, pp 927-939, 1996.
- N. Aretakis, K. Mathioudakis, Wavelet analysis for gas turbine fault diagnostics, *Journal of Engineering for Gas Turbines and Power*, pp 870-876, 1997.
- Computing Vision and Remote Sensing. Berlin University of Technology. Image Analysis. 2009.
- Schoen, R.R., Habetler, T.G., Kamran, F. and Bartheld, R.G. (1995), "Motor bearing damage detection using stator current monitoring", *IEEE Transactions on Industry Applications*, Vol. 31 No. 6, pp. 1274-9.
- G. O. Chandroth, W. J. Staszewski, Fault detection in internal combustion engines using wavelet analysis, in: *Proceedings of COMADEM '99*, Chipping Norton, pp 7-15, 1999.
- C. K. Chui. *An Introduction to Wavelets*, San Diego, CA: Academic Press, 1992.
- Z. K. Peng, F. L. Chu, Application of the wavelet transforms in machine condition monitoring and fault diagnostics: A review with bibliography, *Mechanical Systems and Signal Processing*, pp 199-221, 2004.
- Milan S, Vaclav H, and Roger B. *Image Processing, Analysis, and Machine Vision*. Chapman & Hall computing series. Chapman & Hall Computing, London, 1 edition, 1993.
- L. A. ZADEH. The role of fuzzy logic in the management of uncertainty in expert systems. *Fuzzy Sets and Systems* Volume 11 Issue 1-3, Pages 197-198, 1983.
- Bezdek, J.C., *Pattern Recognition with Fuzzy Objective Function Algorithms*, Models for Pattern Recognition. Plenum Press, New York and London, 1981.
- Hathaway, R.J., Yingkang H. and Bezdek, J.C. Generalized fuzzy C-means clustering strategies using L_p norm distances, *Fuzzy Systems. IEEE Transactions on*, vol 8, issue 5, pp 576-582. 2000.
- Hamed, P. and Leonid, T. Application of Fourier descriptors and fuzzy logic to classification of radar subsurface images, *Proc. SPIE* vol. 5238, Image and Signal Processing for Remote Sensing IX, SPIE, Bellingham, WA, 2004.
- Gabor, B. Matching Features Using Fourier Descriptors. MAPPS/ASPRS 2006 Fall Conference San Antonio, Texas. November 6-10, 2006.
- Abdul Salam. T. H. and Berrached, N.E. 2D Objects Recognition by Invariant Fourier Descriptors. *Journal of Science & Technology* Vol. (8), No (1) 2003.
- Sérgio, O. *Image Processing Techniques Applied to Problems of Industrial Automation*, Instituto Superior Técnico. Lisboa, Portugal, 2006.
- Wang, X. and Xie, K. Application of the Fuzzy Logic in Content-based Image Retrieval. *Journal of Computer Science and Technology (JCS&T)*. Vol. 5 No.1. April 2005.